IF=5.9; Q1

A landscape of circular RNA expression in the human heart

**Wilson L. W. Tan[1,2]†, Benson T. S. Lim[1,2]†, Chukwuemeka G. O. Anene-Nzelu[1,2],
Matthew Ackers-Johnson[1,2], Albert Dashi[1,2], Kelvin See[1], Zenia Tiang[1,2],
Dominic Paul Lee[1], Wee Woon Chua[2], Tuan D. A. Luu[2], Peter Y. Q. Li[2],
Arthur Mark Richards[2], and Roger S. Y. Foo[1,2]***

[1]Genome Institute of Singapore, 60 Biopolis Street, Singapore 138672, Singapore; and [2]Cardiovascular Research Institute, National University Health System, Centre for Translational Medicine, 14 Medical Drive, Singapore 117599, Singapore

Aims	Circular RNA (circRNA) is a newly validated class of single-stranded RNA, ubiquitously expressed in mammalian tissues and possessing key functions including acting as microRNA sponges and as transcriptional regulators by binding to RNA-binding proteins. While independent studies confirm the expression of circRNA in various tissue types, genome-wide circRNA expression in the heart has yet to be described in detail.
Methods and results	We performed deep RNA-sequencing on ribosomal-depleted RNA isolated from 12 human hearts, 25 mouse hearts and across a 28-day differentiation time-course of human embryonic stem cell-derived cardiomyocytes. Using purpose-designed bioinformatics tools, we uncovered a total of 15 318 and 3017 cardiac circRNA within human and mouse, respectively. Their abundance generally correlates with the abundance of their cognate linear RNA, but selected circRNAs exist at disproportionately higher abundance. Top highly expressed circRNA corresponded to key cardiac genes including Titin (*TTN*), *RYR2*, and *DMD*. The most abundant cardiac-expressed circRNA is a cytoplasmic localized single-exon *circSLC8A1-1*. The longest human transcript *TTN* alone generates up to 415 different exonic circRNA isoforms, the majority (83%) of which originates from the I-band domain. Finally, we confirmed the expression of selected cardiac circRNA by RT-PCR, Sanger sequencing and single molecule RNA-fluorescence *in situ* hybridization.
Conclusions	Our data provide a detailed circRNA expression landscape in hearts. There is a high-abundance of specific cardiac-expressed circRNA. These findings open up a new avenue for future investigation into this emerging class of RNA.

1. Introduction

One of the greatest surprises of high-throughput transcriptome analysis in past years is the discovery that our mammalian genome is pervasively transcribed into many different complex families of RNA.[1,2] Among these, microRNAs are now known to regulate virtually all aspects of cardiovascular biology,[3] and promise to be a useful biomarker for disease diagnosis and prognosis.[4] Another class of RNA called long non-coding RNA regulate cardiomyocyte differentiation and pathophysiology,[5,6] fetal gene reprogramming during the myocardial stress–response,[7] and turns out occasionally to code for previously undetected micropeptides that again regulate important aspects of cardiac biology.[8] Overall,

RNA-mediated therapeutics and biomarkers are hotly pursued candidates for cardiovascular disease.[6,9] Circular RNA (circRNA) is yet another newly validated RNA species, now attracting widespread attention.[10–16]

An exonic circRNA is formed when the 5′ end of an exon is covalently back-spliced to its 3′ end, forming an exonic circle (*Figure 1A*). Back-spliced exon–exon junctions curated from high-throughput transcriptome analyses enable the recognition of circRNA as widely expressed abundant RNA species. Formation of circRNA back-spliced junctions is likely to involve the canonical spliceosome, and hence contains the canonical splice site GT/AG signal. Two mechanisms have been proposed which involve either direct back-splicing or 'exon-skipping',[17] and splicing

*Corresponding author. Tel: +65 6601 1036; fax: +65 6872 2998, E-mail: foosyr@gis.a-star.edu.sg
†The first two authors are shared first author.
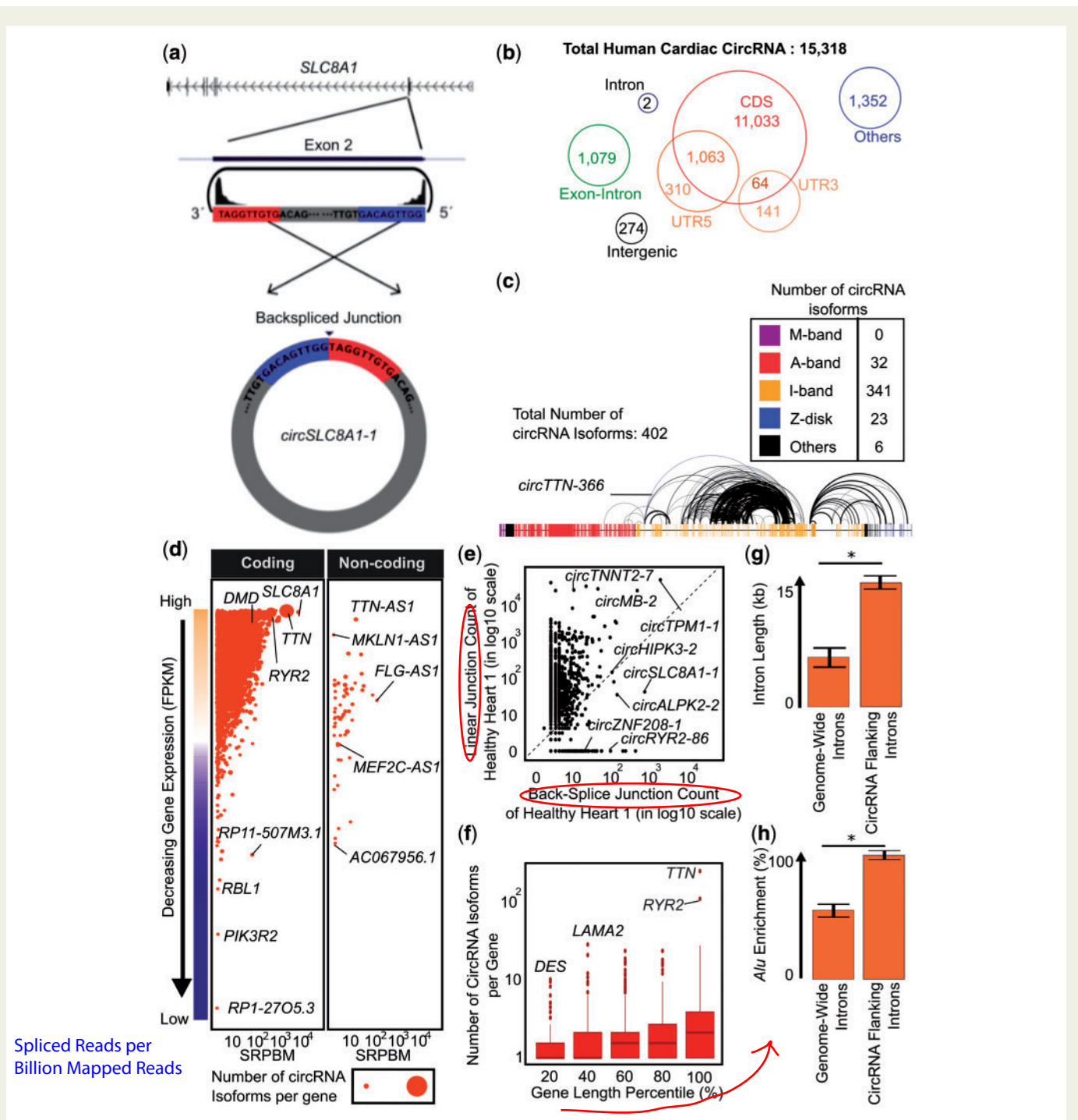
Figure 1 Global landscape of human cardiac circRNA. (A), Schematic showing a sequencing back-spliced junction-read leading to the identity of the single-exon human circRNA *circSLC8A1*. (B), Chart showing circRNA detected in human hearts. (C), A map of circRNA isoforms expressed from the *TTN* gene locus. Larger loops represent back-splice junctions spanning across multiple exons. Note small black loops spanning single or fewer exons, especially in the A-band domain. *circTTN-366* (blue loop) is by prediction the longest cardiac circRNA that spans 153 exons. (D), Integrated panels to show the relationship between linear protein coding or non-coding gene expression and their corresponding circRNA expression. Heatmap shows the average expression of linear genes ranked by expression abundance (highest FPKM: yellow; lowest FPKM: blue). Scatterplots show the expression abundance of circRNA isoforms corresponding to their protein-coding or non-coding linear genes in the rank position of the heatmap. The size of each point in the scatterplots is adjusted according to the number of circRNA isoforms generated by each linear gene. (E), Scatterplot showing the relationship between the abundance of each back-spliced junction representative of the circRNA (x-axis) to their corresponding linear spliced junction representing the linear transcript (y-axis), in a healthy human heart sample. Some genes express significantly more circRNA than their corresponding linear transcript such as *SLC8A1*, *TTN*, and *RYR2*. Otherwise, most genes such as *TPM1 and TNNT2* express more linear transcripts than circRNA. (F), Boxplot showing the relationship between linear gene length and the number of their circRNA isoforms per linear gene. Linear genes were divided into quartiles based on their gene lengths. (G), Barplot showing that introns flanking circRNA are significantly longer than the average intron. *P-value* <0.01. (H), Barplot showing that introns flanking circRNAs are significantly enriched with *Alu* repetitive elements. *P-value* <0.01. *P*-values were obtained by non-parametric bootstrapping.

appears to take place co-transcriptionally.[18] Intronic regions flanking many circRNA are markedly longer and enriched for *ALU* repetitive elements.[19]

The exon–exon back-splice may involve only a single exon (as in *Figure 1A*), forming a single exon circRNA, or in some cases several contiguous exons in the same gene that may be linearly spliced with the most distal 5′ and 3′ exons back-spliced to form a multi-exonic circRNA. It follows that alternative splicing may therefore also affect circRNA isoforms from within the same gene locus. CircRNA that spans exons from neighbouring genes has not been described. Instead, intronic circRNA and circRNA that incorporate exon–intron, also exist.[20,21] Because of its circularity, circRNA lacks an 'open-end' rendering this RNA species resistant to exonuclease RNase-R digestion. Resistance to exonucleolytic RNA decay confers circRNA stability and likely gives circRNA a longer *in vivo* half-life compared with linear forms of RNA such as messenger RNA.[12] Alhasan et al.[22] found that circRNA are 17–188-fold enriched in anucleate human platelets relative to nucleated cells. Degradation resistance is therefore proposed to make circRNA ideal surrogate markers compared with linear RNA in the absence of transcription in platelets.

Independent studies have confirmed the widespread expression of circRNA in different tissues, with contexts of differential expression implicating their biological relevance in some cases.[13,16,23,24] Memczek et al.[11] found 2700 circRNA in tissue from mouse and *Caenorhabditis elegans*. Guo et al.[14] annotated 7112 circRNA from a variety of human cell lines. More recently, Boeckel et al.[25] identified 7388 circRNA in human umbilical vascular endothelial cells (HUVEC). Thousands of highly expressed, stable circRNA show tissue or developmental stage specific expression.[11] One of the first circRNA experimentally validated was the circRNA antisense to the mRNA transcribed from *Sry* (Sex-determining Region Y) locus in rodent testes.[26,27] *circSry* harbours 16 binding sites for miR-138 and thereby functions as a specific miRNA sponge.[27] Another circRNA, arising from the antisense transcript to *CDR1* mRNA (*CDR1as*), also acts as a miRNA sponge to miR-7,[16] although Thomson and Dinger[28] offer skepticism against the generality of the competitive endogenous RNA hypothesis. circRNA may also regulate transcription by direct interaction with RNA-binding proteins.[20] Szabo et al.[29] reported the increasing expression of circRNA from the gene *NCX1* (Na^+/Ca^{++} exchanger, also known as *SLC8A1*) during cardiomyocyte differentiation from human embryonic stem cells (hESC). The genome-wide expression of circRNA in mammalian hearts has been published,[30] but a deeper analysis, also incorporating comparisons across other non-cardiac tissue types is still lacking.

To systematically identify and analyse for cardiac-expressed circRNAs, we deeply sequenced ribosomal-depleted RNA-seq libraries, and filtered specifically for head-to-tail back-spliced exon–exon junction reads. For human, we extracted total RNA from 12 human hearts, which included hearts from healthy normal controls, patients with ischaemic and non-ischaemic dilated cardiomyopathy (ICM and DCM), as well as hypertrophic cardiomyopathy (HCM). We also performed the same procedure for RNA-seq libraries constructed from a differentiation protocol tracking hESC to differentiated cardiomyocytes *in vitro* (D0, 1, 5, 14 and 28). For mouse, we took cardiomyocytes-only isolated from the hearts of mice that had undergone pressure-overload hypertrophy following transverse-aortic constriction (TAC) compared with Sham-operated mice. For validation, we performed Reverse-transcription Polymerase Chain Reactions (RT-PCR), Sanger sequencing and quantitative RT-PCR. Single molecule RNA Fluorescence *In Situ* Hybridization (smRNA-FISH) was also performed for the highly abundant circRNA candidate, *circSlc8a1-1*.

2. Methods

2.1 Human and mouse hearts

Human left ventricular (LV) samples (see Supplementary material online, *Table S1*) were obtained through an IRB protocol approved by the Papworth (Cambridge) Hospital Tissue Bank Review Board and the Cambridgeshire Research Ethics Committee (UK). Written consent was obtained from all individuals according to the Papworth Tissue Bank protocol, conforming to the Declaration of Helsinki. Diseased tissues were from patients undergoing cardiac transplantation for end-stage heart failure, and harvested as previously described.[31,32] Healthy normal LV were from healthy male individuals who had consented to research organ donation through the UK Human Tissue Bank and Ethical Tissue (The ICT Bioincubator, University of Bradford, West Yorkshire, UK). Mouse hearts were harvested for cardiomyocytes-only from TAC- and sham-operated mice, 3 weeks following surgery, as previously described.[33,34] Echo data confirmed consistent pressure-overload hypertrophy in TAC-operated mice (see Supplementary material online, *Table S1*). Animal procedures were carried out on an Institutional Approved protocol for animal use, and conformed to guidelines from Directive 2010/63/EU on the protection of animals used for scientific purposes. Isoflorane 4% mixed with oxygen, was used for inhalation anaesthesia in mice prior to cardiac harvest. Mouse CM-only were harvested according to a recently published method, yielding >95% purity.[35] Samples used for human hearts were based upon availability, whereas sample size for mouse sham/TAC was based upon the anticipated differential expression of coding and non-coding RNA as calculated in Matkovich et al.[36]

2.2 hESC to cardiomyocytes differentiation

The hESC line H1 was maintained using mTeSR media in Matrigel coated tissue culture plates and passaged regularly using a 50/50 mix of dispase and collagenase IV (both at 1 mg/mL). Two days prior to starting differentiation, cells were dissociated using Accutase and seeded as single cells in Matrigel-coated 12-well plates. Differentiation was performed following the published protocol by Lian et al.[37] 10 µM of CHIR99021 was added on day 0 and left for 24 h followed by medium change. 5 µM IWP was added on day 3 and left for 48 h. Culture medium from day 0 to day 7 was RPMI1640 plus B-27 serum-free supplement without insulin. From day 7 and onwards, RPMI1640 with B-27 serum-free supplement (with insulin) was used and changed every 2–3 days.

2.3 Preparation and analysis of ribominus and RNase-R RNA-seq libraries

Samples for RNA-seq were 1 µg in 10 µl, as assessed by the Agilent Bioanalyzer for RNA integrity, prior to library preparation. Library preparation was performed using the Illumina Truseq kit according to manufacturer's protocol. For RNaseR treatment, total RNA was first subjected to large ribosomal RNAs removal using RiboMinus™ Transcriptome Isolation Kit (ThermoScientific) before treatment with RNase R (epicentre) at 3 U of RNase R per µg of RNA. Digested RNA was purified with standard RNA Phenol/Chloroform/Isoamylic alcohol extraction. Sequencing was performed on the Illumina Hiseq2000 high-output with 2×100 sequencing length. Fastq files were aligned to the genomes (*hg19* and *mm9*) using *Tophat2* (version 2.2.0.12) with default parameters.[38] Linear gene expression was computed using *Cufflinks2* (version 2.2.1).[38] Linear gene expression level was reported in Fragment Per Kilobase per Million Reads (FPKM).[38]

2.4 RNA isolation, PCR and qPCR

cDNA templates from reverse transcribed RNaseR-treated samples were PCR amplified using Bio-Rad C1000 touch thermal cyclers and Qiagen HotStarTaq Master Mix using random hexamers and according to manufacturer's protocol. We performed 39 cycles of PCR and used genomic DNA as negative control. PCR products were visualized after gel electrophoresis in 2% ethidium bromide-stained agarose gel. To confirm the PCR results, the PCR products were purified using EXo-AP PCR clean up kit and Sanger capillary sequencing on the purified PCR products was performed by 1st BASE DNA sequencing services (Singapore) using custom designed primers. Quantitative RT-PCR was performed with more than three biological replicates, and all data were normalized to the average expression of *GAPDH* and *18S*. Statistical analysis for differential gene expression was performed using analysis of variance (ANOVA) test. The primers were designed using NCBI Primer-BLAST. All primers and raw CT values were listed in Supplementary material online, *Table S8*.

2.5 Single molecule RNA-FISH in adult mouse cardiomyocytes

Isolated CM adhered onto laminin coated #1 coverslips (ThermoScientific) were fixed for 10 min at r.t.p. with Fixation Buffer (3.7% formaldehyde in PBS), washed twice in 1× PBS and permeabilized with 70% EtOH at 4 °C for at least an hour. Cells were washed with Wash Buffer (10% formamide in 2× SSC) prior to hybridization. RNA FISH was performed using antisense double digoxigenin (DIG) labeled LNA probe ('5DIG_N/CAACTGCTCCAACACTATTTCATCG/3DIG_N') specific to the back-splice junction of *circSlc8a1-1* RNA custom made from Exiqon. An RNA probe antisense to the linear *Slc8a1* transcript was transcribed using TranscriptAid T7 High Yield Transcription Kit (ThermoFisher Scientific), with the corresponding insertion into pCR™II-TOPO® Vector (ThermoFisher Scientific) as a template for transcription, and was labeled with Alexa Fluor488 with the ULYSIS Nucleic Acid Labeling Kit (Invitrogen), which added a Fluor on every G of the probe to amplify the fluorescence intensity. The template for *Slc8a1* was PCR amplified using the following primers: *Slc8a1* Forward: 5′-CAC TTT GGC TGC ACC ATT GG-3′ and *Slc8a1* Reverse: 5′-CGA TTC CCA GGA AGA CAT TCA C-3′. RNA Probes were denatured at 80 °C for 10 min prior to hybridization. RNA and LNA probes were applied onto isolated CM and hybridized for 15–17 h at 37 °C in a humidified chamber After hybridization cells were washed three times in 2× SSC at 42 °C for 10 min. To detect the hybridized anti-*circSlc8a1-1* probes, cells were incubated with a 1:200 dilution of DyLight 594 conjugated goat anti-digoxigenin (Abcam) for 1 h at 37 °C in a humidified chamber. After hybridization cells were washed three times in 2× SSC at 42 °C for 10 min and counterstained with DAPI (5 ng/mL) in between washes. Coverslips were transferred onto glass slides with mounting medium (Vectashield) and imaging was performed on an upright microscope (Nikon Ni-E) with 100× Objective (Nikon) on a cooled CCD/CMOS camera (Qi-1, Qi-2, Nikon). Controls used were no-probe control, and separately, an unrelated 2.2 kb bacterial RNA probe that does not bind to mouse sequences. To demonstrate the specificity of the LNA probe for *circSlc8a1-1* cells were treated with RNase R (10U) for 30 min and then fixed again before being subjected to the above FISH protocol.

2.6 Detection, annotation and quantification of circRNA

RNA-seq data were analysed using an efficient and unbiased *de novo* circRNA identification pipeline known as *CIRI*,[39] with default parameters.

This method detects back-spliced junction reads following the alignment result of Burrows–Wheeler Aligner (BWA-MEM),[40] and performs systematic filtering to exclude false positives. CIRI analyses all alignment records in SAM file generated by BWA-MEM, and looks for potential back-spliced junction reads which are made up of two segments which align to the reference genome in chiastic order. *CIRI* requires the candidate back-spliced junction reads to align in the same chromosome and strand. Unlike the other method used in previous studies,[12,16,18,25,41] *CIRI* takes advantage of the paired-end mapping information for preliminary filtering of false positive back-spliced junction reads by excluding those candidates with its paired reads not mapped within the region of the putative circRNA range. Next, *CIRI* filters candidate junction reads that are not flanked by the canonical splicing signal (GT-AG) nor supported by exon boundaries provided in GENCODE (version 19 for *hg19* and M1 for *mm9*) GTF annotation file. We required our circRNA candidates to be supported by at least two unique back-spliced reads. High-confidence circRNA isoforms were defined as only those that satisfied the further criteria of ones being detected in at least two samples. We annotated our cardiac circRNA candidates to hg19 and mm9 GENCODE (version 19 for *hg19* and M1 for *mm9*).

Relative expression level of circRNA isoforms is quantified in SRPBM (Spliced Reads per Billion Mapped Reads):

$$SRPBM = \frac{x}{n} \times 1\ 000\ 000\ 000$$

where x is the total number of back-spliced junction reads and n is the total number of mapped reads. We use backspliced-to-linear ratio to determine the relative expression of circRNA with respect to the cognate linear mRNA that stems from the same exon.

$$Backspliced - to - linear\ ratio = \frac{c}{\max(l_1, l_2)}$$

where c represents the total back-spliced junction read count that spans both ends of the back-spliced exon (s), l_1 and l_2 represents the total linear read count that spans left and right linear-spliced junctions of the same exon(s), respectively.

2.7 External RNA-seq datasets

rRNA-depleted RNA-seq datasets of various human tissues from ENCODE were used. The ENCODE experimental accession: ENCSR000AEW (cerebellum), ENCSR000AFE (parietal lobe), ENCSR000AFB (liver), ENCSR000AFI (stomach), ENCSR000AFF (skeletal muscle tissue), ENCLB223ZZZ (heart). External rRNA-depleted RNA-seq datasets of human pluripotent-to-cardiomyocytes differentiation were also used (NCBI accession: GSE76523).[42]

3. Results

3.1 Cardiac-expressed circRNAs are derived from highly expressed cardiac protein-coding and non-coding genes

We performed deep RNA-seq on ribosomal-depleted total RNA extracted from a panel of human full-thickness LV myocardial explants comprising of three control hearts, three hearts each from patients with non-ischaemic end-stage heart failure (DCM), and ischaemic end-stage heart failure (ICM), HCM. (see Supplementary material online, *Table S1*, total 12 human hearts). We also undertook the same procedure for cardiomyocytes-only isolated from mouse hearts[35] that developed

pressure-overload hypertrophy following TAC (3 weeks post-TAC) and Sham-operated controls ($N = 12$ for Sham and $N = 13$ for TAC; see Supplementary material online, *Table S1*). Paired-end sequencing reads were aligned to reference genomes (*hg19* for human, *mm9* for mouse) using BWA. Head-to-tail back-spliced junctions were detected using an efficient and unbiased algorithm for *de novo* circRNA identification, *CIRI*.[39] CircRNA were called for each back-splice junction with a minimum coverage of at least two uniquely mapped reads, together with GT/AG splicing signals. *Figure 1A* shows an example of sequencing back-spliced reads leading to the identification of a single-exon circRNA. Supplementary material online, *Table S1* summarizes the tissue information and quality control metrics of sequencing libraries that we generated in this study. We generated an average of 112 million mapped reads per human sample. Majority of the mapped reads were non-spliced reads (85%). ~11% of the total reads were linear spliced reads. Less than 1% of the total reads were back-spliced reads.

In total, we detected 15 318 and 3017 circRNA in human and mouse hearts, respectively (*Figure 1B*, see Supplementary material online, *Figure S1A and Tables S2 and S3*). Among these, 6448 and 1007 were high-confidence exonic circRNA expressed in two or more human and mouse hearts, respectively. Other studies also consistently found more circRNA in human tissue than mouse[11,14,16,41,43]. Even though we had achieved a similar number of uniquely mapped reads from our mouse and human RNA-seq libraries, the number of back-spliced reads and circRNA identified in mouse were significant lower despite using the same algorithm and criteria. For human, we annotated all cardiac circRNA junctions with GENCODE v19 database. 82.32% (12 611/15 318) of the circRNA we identified were derived from exons and generated from individual linear cognate genes. The rest were annotated to exon–intron boundaries (1079/15 318), intron-only (2 out of 15 318: see Supplementary material online, *Table S2*, validated by PCR in Supplementary material online, *Figure S2A*) and others. Majority of the exonic circRNAs were spliced from coding exons (CDS) (96.42%, 12 160/12 611). Similar to human, majority of the mouse cardiac circRNA were exonic (72.35%, 2183/3017) and also mainly annotated to CDS boundaries (2069/2183) (see Supplementary material online, *Figure S1A*). Since RNaseR-treatment of RNA reliably purifies for circRNA species but requires a large quantity of starting RNA material, we compared our circRNA against RNaseR-treated RNA-seq in three DCM hearts and found good reproducibility (see Supplementary material online, *Figure S1B*).

On the basis of back-spliced junctions and existing exon–exon splicing annotation, the median predicted number of exons per cardiac circRNA is four (minimum: 1, average mean: 6, max: 153). The total number of single exonic circRNA was ~8% (1005/12 611), while ~16% (2046/12 611) were predicted to span at least 10 exons (see Supplementary material online, *Table S2*). The longest circRNA was *circTTN-366*, predicted to span 153 exons (see Supplementary material online, *Table 2 and Figure S1C*).

Although the majority of human exonic cardiac circRNAs (95.25%, 12 012/12 611) had an average coverage of less than 10 back-spliced junction reads, 35 highly expressed circRNAs had a high-average read count of more than 50, making them the most highly expressed circRNA in human hearts (*Table 1*, *Figure 1D*). These included *circSLC8A1-1*, *circTPM1-1*, *circTTN-90*, *circTTN-275*, *circHIPK3-2*, *circEXOC6B-14*, *circALPK2-2*, *circMB-2*, *circNEBL-19*, *circMYBPC3-3* and *circRYR2-113*. Non-protein-coding genes also generated a high-number of circRNA (*Figure 1D*). Among the top expressing circRNA from corresponding annotated non-coding linear genes were *circTTN-AS1-1*, *circFLG-AS1-1*, *circMKLN1-AS1-1*, and *circMEF2C-AS1-1*. Consistently, for

Table 1 Top highest expressed circRNA in human hearts

CircRNA	Number of hearts detected (max12)	Predicted number of exons	Average raw junction count
circSLC8A1-1	12	1	2030
circTPM1-1	8	2	792
circTTN-90	9	1	536
circTTN-275	8	1	250
circHIPK3-2	12	1	226
circEXOC6B-14	12	4	208
circALPK2-2	12	1	177
circTTN-155	5	1	168
circMB-2	12	1	168
circTTN-88	10	67	151
circZNF91-4	12	1	144
circMYL2-2	1	2	123
circNEBL-19	8	2	114
circRYR2-86	9	1	113
circNEBL-23	12	1	102
circARHGAP5-1	12	2	101
circTTN-344	10	57	98
circRYR2-113	12	12	96
circN4BP2L2-8	12	4	93
circTTN-81	10	2	88
circMYH7-4	2	1	86
circTTN-216	8	1	80
circTECRL-11	12	6	82
circNRAP-1	11	1	74
circRHOBTB3-14	12	2	72
circKLHL24-8	12	6	72
circMYBPC3-3	12	4	70
circARHGAP5-6	12	1	63
circTTN-57	10	2	60

protein-coding genes, but seemingly not for non-coding genes, we noted that linear genes with the highest expression produced proportionally the highest abundance of circRNA (*Figure 1D*). 30 of the top 100 most highly expressed linear cardiac genes produced at least one circRNA isoform each, including *MYL2*, *TPM1*, *DES*, *MB*, *MYH7*, *TTN*, *FHL2*, and *TNNT2* (*Table 2*). On the other hand, top cardiac-expressed linear genes that did not produce any circRNA included *ACTC1*, *MYL12A*, *NPPA*, and *TCAP*. Expression abundance of circRNA-producing linear genes was significantly higher than linear genes that did not produce detectable circRNA (average FPKM of circRNA-producing linear genes: 120.98; average FPKM of other genes: 12.20; Wilcoxon rank sum test with continuity correction *P*-value $< 2.2 \times 10^{-16}$). Linear genes that were not expressed in the heart did not generally show any expression of corresponding circRNA (*Figure 1D*). Remarkable exceptions to this were *RBL1*, *PIK3R2* and *RP1-27O5.3*. These were non-cardiac-expressed linear protein-coding genes that generated circRNA in the heart, at least in our analysis. The most abundant human cardiac-expressed circRNA by far was a single-exon circular isoform from the Na^{+}/Ca^{++} exchanger gene *SLC8A1*, also known as *NCX1*, with an average of 2030 back-spliced junction reads across all human heart samples (*Table 1*, *Figure 1D*). In mouse cardiomyocytes, the same exon in *Slc8a1* also generated the 2nd most abundant mouse cardiomyocyte circRNA (*circSlc8a1-1*, *Table 3*). Other

Table 2 Number of circRNA isoforms expressed by top expressed linear genes in human hearts

Gene	Average FPKM for linear gene	Number of circRNA isoforms
MYL2	9554.09	3
TPM1	6464.53	7
DES	5236.68	18
TNNI3	4928.40	3
MB	4777.38	2
MYH7	3993.61	26
TNNT2	3619.52	18
CRYAB	3405.40	2
TNNC1	3206.41	1
ACTC1	2875.12	0
MYL3	2475.83	1
ANKRD1	2362.68	4
ACTA1	2360.67	2
FABP3	2261.20	0
MYL12A	2241.37	0
TPT1	2080.82	1
RPL37A	1438.20	0
NPPA	1357.58	0
COX7C	1349.62	0
RPS27	1340.15	0
GAPDH	1338.99	0
PTGDS	1302.89	1
CKM	1258.61	3
RPL41	1225.52	0
ATP5B	1223.01	0
TTN	1166.64	401
B2M	1163.78	0
TCAP	1098.13	0
UQCRB	1076.40	0
COX7A1	1049.55	0

Table 3 Top highest expressed circRNA in mouse hearts

CircRNA	Number of hearts detected (max 25)	Predicted number of exons	Average raw junction count
circTtn-63	25	34	172
circSlc8a1-1	25	1	132
circTpm1-3	11	2	110
circAtp2a2-1	13	1	104
circTtn-37	25	35	56
circMyh6-7	9	1	59
circMyl2-3	1	4	34
circTulp4-3	25	1	21
circTtn-32	25	7	19
circTpm1-4	1	5	27
circTnnt2-10	8	1	28
circMyh6-4	8	2	19
circMsrb3-1	25	4	10
circRyr2-3	25	4	10
circStrn3-4	25	6	10
circTnnt2-3	1	3	15
circFhl2-1	23	2	9
circNfix-3	24	1	10
circTtc3-4	25	11	8
circMettl9-2	24	3	7
circOgdh-3	23	3	9
circHipk3-1	23	1	9
circElf2-3	23	3	8
circMyocd-2	23	6	7
circQk-1	23	3	6
circTtn-56	7	52	9
circZfp644-6	23	5	6
circCpeb3-4	22	3	6
circLrch3-2	25	6	6
circPhf21a-1	23	5	5

top expressed circRNA in mouse cardiomyocytes are listed in *Table 3*. For all genes, linear junctions largely outnumbered corresponding back-spliced junctions (e.g. circTPM1-1 and circTNNT2-12 in *Figure 1E*), but in some prominent cases, such as *circSLC8A1-1*, the back-spliced junction was up to 40 times more abundant than the corresponding linear junction, suggesting that the *circSLC8A1-1* is more abundant than linear *SLC8A1* transcripts, at least based on assessment at this spliced junction (*Figure 1E*). We further determined that this spectrum of backsplice-to-linear ratio is consistent and reproducible across different hearts (average spearman correlation rank, r=0.85, P-value <0.001) (see Supplementary material online, *Figure S1D*).

3.2 The longest human linear mRNA *TTN* has the largest number of circRNA isoforms

On average, each circRNA-producing linear gene generated three circRNA isoforms (see Supplementary material online, *Table S4*). Two important cardiac genes produced more than 100 circRNA isoforms each: *TTN* (401 exonic circRNA isoforms, *Figure 1C*) and *RYR2* (177 circRNA

isoforms) (*Figure 1F*, *Table 4*). The same was found in mouse cardiomyocytes (*Table 5*, see Supplementary material online, *Table S4*). Non-sense or frameshift mutations in the *TTN* A-band domain leading to *TTN* protein truncations were recently implicated as a major cause for DCM.[44,45] We found 32 circRNA isoforms generated from within the A-band domain of *TTN*, but interestingly, a large diverse variety of multi-exon circRNA were generated from the I-band, which is the domain of *TTN* known to be most heavily linear spliced (*Figure 1C*). In general, longer linear genes correlated with more circRNA isoforms, although again, exceptions were *DES* and *LAMA2* which are shorter genes (6 kb and 20 kb, respectively) that generated 18 and 47 circRNA isoforms each (*Figure 1F*).

3.3. Features in introns flanking cardiac-expressed circRNA

Others had observed that flanking intron lengths correlated with the production of circRNA.[12,17] In our shortlist of cardiac-expressed circRNA, we confirmed that the average length of circRNA-flanking introns was significantly longer than genome-wide average intron length (median circRNA-flanking intron length: 7451; genome-wide average

Table 4 Linear genes and transcript-lengths with the top highest number of circRNA isoforms expressed in human hearts

Gene	Linear transcript length (nt)	Number of exons in linear gene	Number of circRNA
TTN	1 177 337	3416	401
RYR2	103 021	690	177
NEBL	37 396	161	48
LAMA2	20 518	145	47
DMD	177 903	1019	43
AKAP13	100 068	380	41
ANKRD36C	47 483	657	40
BIRC6	42 530	211	38
PTK2	161 184	1263	38
NBAS	48 123	347	37
NBPF10	66 391	474	33
VPS8	65 210	613	33
VWA8	22 211	159	33
ARHGAP10	27 499	145	32
MYOM1	36 955	264	30
ANKRD36	35 391	345	29
FOCAD	43 659	340	29
LTBP1	88 997	573	29
MLIP	43 734	244	29
PXDNL	27 870	125	27
AGTPBP1	43 934	302	26
MYH7	12 180	84	26
NBPF20	44 647	320	26
VPS13B	112 005	547	26
PDLIM5	68 502	373	24
TMEM245	28 607	108	24
TRDN	28 991	230	24
PPP6R3	108 310	667	23
UBAP2	65 615	443	23
BPTF	120 441	401	22

Table 5 Linear genes and transcript-lengths with the top highest number of circRNA isoforms expressed in mouse hearts
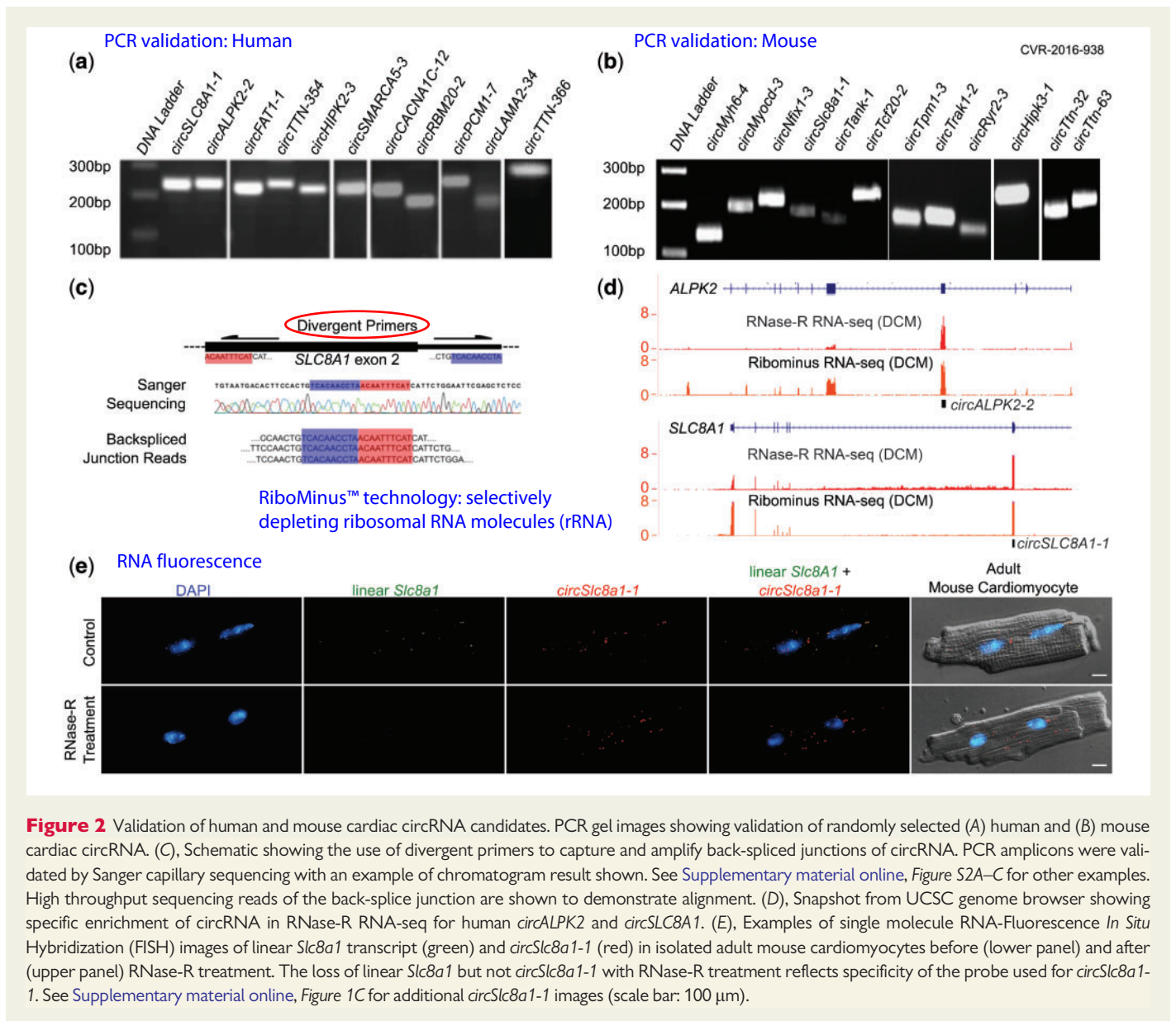
Gene	Linear transcript length (nt)	Number of exons in linear gene	Number of circRNA
Ttn	1 228 948	4046	78
Ryr2	43 482	268	22
Myh6	22 258	166	16
Tnnt2	8686	130	13
Obscn	217 183	940	13
Asph	114 042	530	11
Arhgap10	17 808	146	11
Zfp644	61 060	154	9
Trdn	13 469	128	9
Clasp1	46 332	250	8
Ccdc141	32 143	141	8
Myl2	10 701	132	8
Ubn2	72 691	167	8
Cacna1c	73 995	461	8
Agtpbp1	93 482	633	8
Arhgap26	65 248	261	8
Cpeb3	87 587	272	8
Sorbs1	47 641	455	8
DMD	82 145	438	8
Corin	27 218	138	7
Erc1	28 002	101	7
Scaper	36 337	250	7
Canx	9106	43	7
Slmap	78 809	443	7
1110028C15Rik	32 885	120	6
Mllt10	47 869	267	6
Rere	39 043	149	6
Phkb	29 945	237	6
Tpm1	57 428	389	6
Ttc3	117 060	927	6

intron length: 1567; non-parametric resampling P-value <0.01; Figure 1G). Similarly, we observed that flanking introns were significantly enriched with Alu repeats elements (percentage enrichment for introns flanking circRNA: 88%; global percentage enrichment of Alu elements in intron: 49%; non-parametric resampling bootstrap P-value <0.01; Figure 1H). Flanking introns of the most abundantly expressed circRNA, circSLC8A1-1, are unusually long (250 618 nt) and are enriched with Alu elements. Again as exception, we noted that some highly expressed cardiac circRNAs have neither long flanking intronic lengths nor Alu element enrichment. One such example is circTPM1-1, whose left intron length is 942 nt, right intron length is 1419 nt, and is without any Alu element in either flanking intron.

3.4 Validation of cardiac-expressed circRNA candidates

To validate our shortlist of cardiac-expressed circRNA, we randomly selected 30 human and 20 mouse candidates from a range of high,

moderate and low-expression levels as determined by our RNA-seq junction read-count analysis. From these, we definitively confirmed the back-spliced structure of 24/30 and 19/20 of human and mouse cardiac circRNA candidates by RT-PCR using junction-specific divergent primers and Sanger sequencing (Figures 2A–C, see Supplementary material online, Figure S2B and C). We also performed PCR on the respective genomic DNA using the corresponding divergent primers, and confirmed that back-spliced junctions were in RNA transcripts and not due to genomic exon reshuffling or tandem duplications. By performing the same RT-PCR on RNase-R treated RNA samples, we further confirmed that back-spliced products were present in RNA circles. We also compared linear and backspliced PCR products by using convergent and divergent primers, respectively, and RT by using oligo-dT or random hexamers, and further confirmed the circularity of candidates (see Supplementary material online, Figure S2D). Using single molecule RNA-FISH, we established the cytoplasmic localization of circSlc8a1-1 in adult mouse cardiomyocytes (Figure 2D and see Supplementary material online, Figure S2E).

Figure 2 Validation of human and mouse cardiac circRNA candidates. PCR gel images showing validation of randomly selected (A) human and (B) mouse cardiac circRNA. (C), Schematic showing the use of divergent primers to capture and amplify back-spliced junctions of circRNA. PCR amplicons were validated by Sanger capillary sequencing with an example of chromatogram result shown. See Supplementary material online, *Figure S2A–C* for other examples. High throughput sequencing reads of the back-splice junction are shown to demonstrate alignment. (D), Snapshot from UCSC genome browser showing specific enrichment of circRNA in RNase-R RNA-seq for human *circALPK2* and *circSLC8A1*. (E), Examples of single molecule RNA-Fluorescence *In Situ* Hybridization (FISH) images of linear *Slc8a1* transcript (green) and *circSlc8a1-1* (red) in isolated adult mouse cardiomyocytes before (lower panel) and after (upper panel) RNase-R treatment. The loss of linear *Slc8a1* but not *circSlc8a1-1* with RNase-R treatment reflects specificity of the probe used for *circSlc8a1-1*. See Supplementary material online, *Figure 1C* for additional *circSlc8a1-1* images (scale bar: 100 μm).

3.5 Heart-specificity of cardiac-expressed circRNA candidates and lack of differential expression of circRNA in human diseased hearts

Next we downloaded tissue RNA-seq datasets from the ENCODE Project Consortium and analysed with the same algorithm for unbiased comparison against our cardiac circRNA shortlist. We identified 1664 cardiac-specific circRNA which were detected in hearts only (see Supplementary material online, *Figure S2A*). Gene ontology confirmed that these heart-specific circRNAs are highly enriched for cardiac-specific biological processes (adjusted P-value $<1 \times 10^{-5}$) including cytoskeleton organization, actin-mediated cell contraction, muscle filament sliding, cardiac muscle contraction and myofibril assembly (see Supplementary material online, *Table S5*), and they corresponded largely genes that are similarly cardiac-specific (see Supplementary material online, *Figure S2A*). Conversely, other cardiac-expressed circRNA are commonly expressed in other organs. This included the most abundant cardiac *circSLC8A1-1*, which was also highly expressed in skeletal muscle, liver, stomach,

temporal lobe and cerebellum (see Supplementary material online, *Figure S2A*).

Next we asked whether cardiac circRNA were differentially expressed between healthy and diseased hearts. Analysis based on junction count from our dataset did not yield any differentially expressed candidates with strong statistical significance. Similarly using the panel of primers that we employed for validating the 24 candidates above, we found that circRNA expression was largely stable across all our human heart samples (see Supplementary material online, *Figure S2B*). Similarly, in Sham- and TAC-operated mouse hearts, we also did not detect any significant circRNA differential expression (see Supplementary material online, *Figure S2C*), despite characteristic changes of stress–response linear genes such as *Nppa*, *Nppb*, and *Myh7*.

3.6 CircRNA expression in the time-course of cardiomyocyte differentiation

In addition to assessing normal and diseased heart tissue, we also turned our attention to circRNA in the differentiation time-course of hESC to
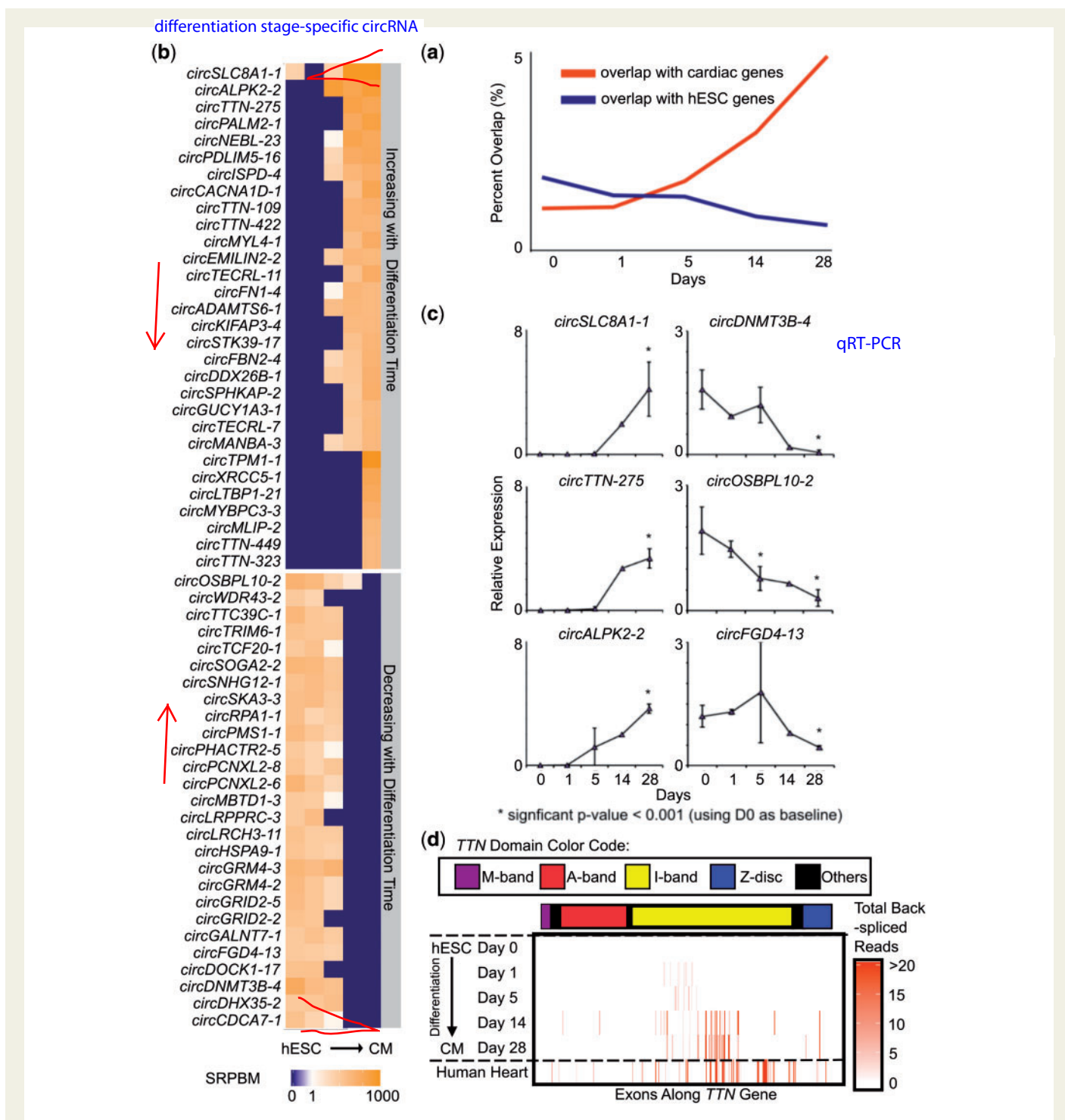
Figure 3 hESC differentiation stage-specific circRNA. (A), Plots showing the overlap of cardiac-specific (red) and D0 hESC-expressed (blue) circRNA at each time point. (B), Heatmap showing the expression changes of circRNA across the hESC differentiation time-course. D0: hESC; D1: precardiac mesodermal progenitors; D5: cardiac progenitors; D14 and D28: immature cardiomyocytes. (C), Quantitative RT-PCR validation of circRNA candidates across the differentiation time-course in three biological replicates. *P*-values obtained by ANOVA test. (D), Heatmap showing increasing number of back-spliced junction reads in the *TTN* locus across the hESC differentiation time-course. Majority of *TTN* circRNA (26/30) expressed in D28 hESC-cardiomyocytes are from the I-band, similar to the observation in human adult hearts.

hESC-cardiomyocytes. In this dataset, we found a total of 6853 exonic circRNAs across all five time-points (see Supplementary material online, *Table S6*). We made a comparison between circRNA expressed in the time-course and adult human cardiac-expressed circRNA curated from above, and found an increasing overlap with cardiac-expressed circRNA,

and decreasing overlap with D0 hESC-expressed circRNA across the progressive time-points (*Figure 3A*). CircRNA expressed in hESC-cardiomyocytes furthest along in the differentiation protocol (on D28, *Figure 3B*) were originating from host genes that were statistically enriched for contractile fiber cellular components such as contractile

fiber (26 genes, adjusted *P*-value = 2 × 10⁻⁴), and myofibril (26 genes, adjusted *P*-value = 3 × 10⁻⁴) (see Supplementary material online, *Table S7*). 479 circRNAs had strong positive correlation with the differentiation time-course (*r* > 0.75, *P*-value <2.2 × 10⁻²²; top candidates shown in *Figure 3B*). These circRNA mapped to genes significantly enriched in GO terms such as heart development (21 genes, adjusted *P*-value = 5.9 × 10⁻³) and anatomical structural development (55 genes, adjusted *P*-value = 8.4 × 10⁻³). Examples of circRNA with increasing abundance over the time-course were: *circSLC8A1-1*, *circTTN-275* and *circALPK2-1*, which we validated by quantitative RT-PCR (*Figure 3C*). Reflecting the significant abundance of these circRNA, each was covered by >100 back-spliced junction-reads on D28. On the other hand, 181 circRNAs showed strong negative correlation with the differentiation time-course (*r* < 0.75, *P*-value < 2.2 × 10⁻²²; top candidates shown in *Figure 3B*). These circRNAs are significantly enriched in cellular metabolic processes (101 genes, adjusted *P*-value = 5 × 10⁻⁴), and included *circDNMT3B-4*, *circOSBPL10* and *circFGD4-7* (*Figure 3C*). We further validated this set of time-course dependent circRNA changes in an independent analysis using a previously published RNAseq of hESC and hESC-cardiomyocytes[42] (see Supplementary material online, *Figure S3*). Coherent with acquiring circRNA that are cardiac-specific, we also found an increase in *TTN* circRNA isoforms in the progressive differentiation from hESC to hESC-cardiomyocytes (*Figure 3D*). At D0, there were no circRNA expressed from the *TTN* loci. The number of *circTTN* increased along the differentiation time course. At D28, the majority of the circRNA were derived from the I-band (26/30), similar to the observation in adult human hearts.

4. Discussion

Just as thousands of non-coding RNA turned out to be transcribed from what was thought to be ancestral sequences or 'junk DNA' across the human genome,[46] 'scrambled exons' first reported in 1991[47] are now recognized as bona-fide back-spliced junctions of abundant and widely expressed circRNA. Datasets of cardiac circRNA expression were recently published.[48,49] Our work now extends the genome-wide analysis to deeper detail. We describe the full spectrum of cardiac circRNA expression corresponding to their cognate cardiac-expressed linear protein coding and non-coding genes. 36 of the top 100 cardiac-expressed linear genes express at least one isoform of circRNA. Generally, the most highly expressed linear genes also have the highest expression abundance of corresponding circRNA, consistent with a biogenesis mechanism that incorporates both linear and circRNA isoforms concurrently from the same gene locus. However, circRNA can also originate very rarely from the loci of non-cardiac-expressed linear genes such as *RBL1* and *PIK3R2*, suggesting the possibility of a unique circRNA biogenesis mechanism that remains to be proven. Similarly, there are some circRNA whose abundance appears to significantly exceed their corresponding linear RNA (e.g. *circSLC8A1-1*), again suggesting the possibility of a disconnect between linear and circRNA biogenesis, or a prolonged stability of the circRNA compared with its linear RNA gene product. Conversely, there are also highly expressed linear cardiac genes such as *ACTC1* and *NPPA* that do not appear to generate any circRNA.

4.1 *circSLC8A1* and *circTTN* isoforms

Regardless of their mechanism of biogenesis or how their expression abundance might be regulated, our study reports a few key discoveries for cardiac circRNA. The most abundant circRNA in human hearts is a single-exon isoform generated from exon 2 of the Na⁺/Ca⁺⁺ exchanger gene, *SLC8A1* (or *NCX1*). Arising from the same exon in mouse, *circSlc8a1-1* is also abundantly expressed in mouse cardiomyocytes. In fact Li and Lytton[50] made the prescient discovery of this circRNA before and showed evidence that this circRNA may encode a 602-amino acid truncated NCX1 protein. Translation of circular transcripts has been reported previously[50] and may reflect a potential physiological function for *circSLC8A1-1*. However, in general, only linear but not circular forms of RNA are present in heavy polyribosome cell fractions,[41] implying that circRNA are not usually translated. Our finding of the near-exclusive cytoplasmic localization of *circSLC8A1-1* in the cardiomyocyte nonetheless suggests that its role is likely to be extra-nuclear. Indeed all circRNA are predominantly cytoplasmic localized.[12] The role of *circSLC8A1-1* will need further assessment by knockdown that targets the circRNA but not its linear transcript.

Another observation from our study is that the longest human transcript *TTN* also has the largest number of circRNA isoforms (402 in total) in the heart, followed by 177 circRNA isoforms encoded by another long cardiac gene *RYR2*. By far the majority of *TTN* circRNA arise from the *TTN* locus encoding the protein I-band domain, upstream of the A-band domain, which is in turn the major site of disease-causing non-sense and frameshift mutations.[44,45] Among its domains, the *TTN* I-band is known to be the most heavily spliced, so it remains possible that the multi-exonic large spectrum of circRNA isoforms in the I-band are mechanistically linked to the abundance of linear splicing in this domain. It would be of interest to know if the expression of *TTN* I-band domain circRNA isoforms is significantly perturbed in patients with disease-causing *TTN* mutations, and if so, whether this influences disease onset or progression. Cardiac biopsies from patients with DCM will be needed to investigate these possibilities. None of our patient samples harboured *TTN* non-sense or frameshift mutations. The production of *DMD* RNA circularization in the presence of a *DMD* frameshift mutation has been associated with a more severe phenotype for muscular dystrophy.[51] We also detected 43 *DMD* circRNA isoforms in our samples of human hearts. Expression levels of the full spectrum of *DMD* circRNA isoforms will also merit further investigation in patients with Duchenne or Beckers muscular dystrophy.

4.2 Differential expression of circRNA in healthy and diseased hearts, and in cardiomyocyte differentiation

From back-spliced junction analysis of our human hearts, we did not find any statistically significant circRNA that were differentially expressed in disease. Indeed even with our sham- and TAC-operated mouse hearts, we did not find any significant differential circRNA expression. Differential expression was instead significant in the progression of cardiomyocyte differentiation. All together, this is reminiscent of the finding reported by Matkovich *et al.*[36] where lncRNA were regulated as a major factor during the developmental transition between late embryonic and adult hearts, but not for the maladaptive compensation that distinguishes normal from pathological diseased hearts in the adult. Interestingly, Du *et al.*[52] found that a candidate circRNA, *circFoxo3*, was highly expressed in hearts of aged patients and mice. Moreover, silencing *circFoxo3* inhibited senescence of mouse embryonic fibroblasts, whereas ectopic expression of circFoxo3 induced senescence. Our own findings of the lack of differential expression between age-matched healthy and diseased hearts will need further study for replication. The lack of circRNA differential expression in disease progression may be a reflection of their

long half-life and stability compared with linear transcripts. Eunuka et al.[53] reported that circRNA in EGF-stimulated cells were stably expressed whereas mRNA and miRNA changed within minutes; and proposed the explanation to be the long half-lives of circRNA. Conversely, an important limitation we may have faced is the lack of sequencing depth for detecting circRNA differential expression given our limitation with back-spliced junction reads. On the basis of our dataset, however, it would now be possible to design targeted back-splice array panels to assess circRNA expression in closer detail, or RNaseR RNA-seq if the starting quantity of RNA is not limiting. In contrast, at a similar sequencing depth, there was significant differential expression of circRNA in the hESC differentiation time-course. The range of circRNA differential expression may therefore be wider in cardiomyocyte differentiation than in health and disease comparisons.

Even if cardiac circRNA are stably expressed and not differentially expressed in disease, a cell-type signature of circRNA expression coupled to its exonucleolytic-resistance and enhanced stability still mean that if carefully selected, circRNA may be attractive candidates for cell-identity biomarkers. Wang et al.[54] showed that the circRNA100783 is a novel biomarker for tracking immune cell ageing or immunosenescence. Indeed circRNA are also found enriched in circulating exosomes.[10] Hence, circRNA that are not differentially expressed but cardiomyocyte-specific could still be robust circulating biomarkers of disease that reflect cardiomyocyte death or myocardial damage, just as Troponin peptides are good biomarkers even though they are not differentially expressed in the myocardium during myocardial infarction. Our analysis has identified 1664 cardiac-expressed circRNA that are heart specific.

4.3 circRNA may serve important biological functions in the cardiovascular system

In another cardiovascular relevant context, a circRNA of the long non-coding RNA *ANRIL* at the chromosome 9p21.3 locus correlates with atherosclerosis risk alleles and expression of the nearby coding gene *INK4/ARF*.[55] Splice prediction algorithms identified polymorphisms in the risk interval that may regulate *ANRIL* splicing and *circANRIL* production,[55] but it remains to be shown how these alternative RNA isoforms directly contribute to disease. Boeckel et al.[25] identified a set of hypoxia-induced circRNA expressed in human umbilical venous endothelial cells. Silencing of *cZNF292* reduced tube formation and spheroid sprouting *in vitro*, implicating a pro-angiogenic role for *cZNF292*.[25] A circRNA (*HRCR*) acts as a miR-223 sponge to inhibit cardiac hypertrophy and heart failure.[56] Hundreds of circRNA are regulated during human epithelial mesenchymal transition (EMT) and the increase in circRNA formation during EMT seems to be regulated by the RNA binding protein QKI.[57] We also found expression of *circQKI* in human hearts.

In summary, much work lies ahead to elucidate mechanisms of action and detailed functional relevance for the different cardiac-expressed circRNA isoforms that we have now catalogued. Our dataset forms an important human heart resource that gives the first detailed overview to the expression landscape of this emerging class of RNA and lays the foundation for future new discoveries into their role in human cardiovascular biology.

Supplementary material

Supplementary material is available at *Cardiovascular Research* online.

Conflict of interest: none declared.

References

1. Djebali S, Davis CA, Merkel A, Dobin A, Lassmann T, Mortazavi A, Tanzer A, Lagarde J, Lin W, Schlesinger F, Xue C, Marinov GK, Khatun J, Williams BA, Zaleski C, Rozowsky J, Roder M, Kokocinski F, Abdelhamid RF, Alioto T, Antoshechkin I, Baer MT, Bar NS, Batut P, Bell K, Bell I, Chakrabortty S, Chen X, Chrast J, Curado J, Derrien T, Drenkow J, Dumais E, Dumais J, Duttagupta R, Falconnet E, Fastuca M, Fejes-Toth K, Ferreira P, Foissac S, Fullwood MJ, Gao H, Gonzalez D, Gordon A, Gunawardena H, Howald C, Jha S, Johnson R, Kapranov P, King B, Kingswood C, Luo OJ, Park E, Persaud K, Preall JB, Ribeca P, Risk B, Robyr D, Sammeth M, Schaffer L, See LH, Shahab A, Skancke J, Suzuki AM, Takahashi H, Tilgner H, Trout D, Walters N, Wang H, Wrobel J, Yu Y, Ruan X, Hayashizaki Y, Harrow J, Gerstein M, Hubbard T, Reymond A, Antonarakis SE, Hannon G, Giddings MC, Ruan Y, Wold B, Carninci P, Guigo R, Gingeras TR. Landscape of transcription in human cells. *Nature* 2012;**489**:101–108.
2. Carninci P. The transcriptional landscape of the mammalian genome. *Science* 2005;**309**:1559–1563.
3. Quiat D, Olson EN. Review series MicroRNAs in cardiovascular disease: from pathogenesis to prevention and treatment. *J Clin Invest* 2013;**123**:11–18.
4. Mayr M, Zampetaki A, Kiechl S. MicroRNA biomarkers for failing hearts? *Eur Heart J* 2013;**34**:2782–2783.
5. Thum T, Condorelli G. Long noncoding RNAs and microRNAs in cardiovascular pathophysiology. *Circ Res* 2015;**116**:751–762.
6. Thum T. MicroRNA therapeutics in cardiovascular medicine. *EMBO Mol Med* 2012;**4**:3–14.
7. Han P, Li W, Lin C-H, Yang J, Shang C, Nurnberg ST, Jin KK, Xu W, Lin C-Y, Lin C-J, Xiong Y, Chien H-C, Zhou B, Ashley E, Bernstein D, Chen P-S, Chen H-SV, Quertermous T, Chang C-P. A long noncoding RNA protects the heart from pathological hypertrophy. *Nature* 2014;**514**:102–106.
8. Anderson DM, Anderson KM, Chang CL, Makarewich CA, Nelson BR, McAnally JR, Kasaragod P, Shelton JM, Liou J, Bassel-Duby R, Olson EN. A micropeptide encoded by a putative long noncoding RNA regulates muscle performance. *Cell* 2015;**160**:595–606.
9. Rooij E van, Olson EN. MicroRNA therapeutics for cardiovascular disease: opportunities and obstacles. *Nat Rev Drug Discov* 2012;**11**:860–872.
10. Li Y, Zheng Q, Bao C, Li S, Guo W, Zhao J, Chen D, Gu J, He X, Huang S. Circular RNA is enriched and stable in exosomes: a promising biomarker for cancer diagnosis. *Cell Res* 2015;**25**:981–984.
11. Memczak S, Jens M, Elefsinioti A, Torti F, Krueger J, Rybak A, Maier L, Mackowiak SD, Gregersen LH, Munschauer M, Loewer A, Ziebold U, Landthaler M, Kocks C, Noble F le, Rajewsky N. Circular RNAs are a large class of animal RNAs with regulatory potency. *Nature* 2013;**495**:333–338.
12. Jeck WR, Sorrentino J a, Wang K, Slevin MK, Burd CE, Liu J, Marzluff WF, Sharpless NE. Circular RNAs are abundant, conserved, and associated with ALU repeats. *RNA* 2013;**19**:141–157.
13. Salzman J, Gawad C, Wang PL, Lacayo N, Brown PO. Circular RNAs are the predominant transcript isoform from hundreds of human genes in diverse cell types. *PLoS ONE* 2012;**7**.
14. Guo JU, Agarwal V, Guo H, Bartel DP. Expanded identification and characterization of mammalian circular RNAs. *Genome Biol* 2014;**15**:409.
15. Valdmanis PN, Kay MA. The expanding repertoire of circular RNAs. *Mol Ther* 2013;**21**:1112–1114.
16. Rybak-Wolf A, Stottmeister C, Glažar P, Jens M, Pino N, Giusti S, Hanan M, Behm M, Bartok O, Ashwal-Fluss R, Herzog M, Schreyer L, Papavasileiou P, Ivanov A, Öhman M, Refojo D, Kadener S, Rajewsky N. Circular RNAs in the mammalian brain are highly abundant, conserved, and dynamically expressed. *Mol Cell* 2015;**58**:870–885.
17. Vicens Q, Westhof E. Biogenesis of circular RNAs. *Cell* 2014;**159**:13–14.
18. Ashwal-Fluss R, Meyer M, Pamudurti NR, Ivanov A, Bartok O, Hanan M, Evantal N, Memczak S, Rajewsky N, Kadener S. CircRNA biogenesis competes with Pre-mRNA splicing. *Mol Cell* 2014;**56**:55–66.
19. Ivanov A, Memczak S, Wyler E, Torti F, Porath HT, Orejuela MR, Piechotta M, Levanon EY, Landthaler M, Dieterich C, Rajewsky N. Analysis of intron sequences reveals hallmarks of circular RNA biogenesis in animals. *Cell Rep* 2015;**10**:170–177.
20. Li Z, Huang C, Bao C, Chen L, Lin M, Wang X, Zhong G, Yu B, Hu W, Dai L, Zhu P, Chang Z, Wu Q, Zhao Y, Jia Y, Xu P, Liu H, Shan G. Exon–intron circular RNAs regulate transcription in the nucleus. *Nat Struct Mol Biol* 2015;**22**:256–264.
21. Zhang Y, Zhang XO, Chen T, Xiang JF, Yin QF, Xing YH, Zhu S, Yang L, Chen LL. Circular intronic long noncoding RNAs. *Mol Cell* 2013;**51**:792–806.

22. Alhasan AA, Izuogu OG, Al-Balool HH, Steyn JS, Evans A, Colzani M, Ghevaert C, Mountford JC, Marenah L, Elliott DJ, Santibanez-Koref M, Jackson MS. Circular RNA enrichment in platelets is a signature of transcriptome degradation. *Blood* 2016;**127**:e1–e11.

23. Salzman J, Chen RE, Olsen MN, Wang PL, Brown PO. Cell-type specific features of circular RNA expression. *PLoS Genet* 2013;**9**.

24. Venø MT, Hansen TB, Venø ST, Clausen BH, Grebing M, Finsen B, Holm IE, Kjems J. Spatio-temporal regulation of circular RNA expression during porcine embryonic brain development. *Genome Biol* 2015;**16**:245.

25. Boeckel J-N, Jaé N, Heumüller AW, Chen W, Boon RA, Stellos K, Zeiher AM, John D, Uchida S, Dimmeler S. Identification and characterization of hypoxia-regulated endothelial circular RNA. *Circ Res* 2015;**117**:884–890.

26. Capel B, Swain A, Nicolis S, Hacker A, Walter M, Koopman P, Goodfellow P, Lovell-Badge R. Circular transcripts of the testis-determining gene Sry in adult mouse testis. *Cell* 1993;**73**:1019–1030.

27. Hansen TB, Jensen TI, Clausen BH, Bramsen JB, Finsen B, Damgaard CK, Kjems J. Natural RNA circles function as efficient microRNA sponges. TL-495. *Nature* 2013;**495**:384–388.

28. Thomson DW, Dinger ME. Endogenous microRNA sponges: evidence and controversy. *Nat Publ Gr* 2016;**17**:272–283.

29. Szabo L, Morey R, Palpant NJ, Wang PL, Afari N, Jiang C, Parast MM, Murry CE, Laurent LC, Salzman J. Statistically based splicing detection reveals neural enrichment and tissue-specific induction of circular RNA during human fetal development. *Genome Biol* 2015;**16**:126.

30. Werfel S, Nothjunge S, Schwarzmayr T, Strom T, Meitinger T, Engelhardt S. Characterization of circular RNAs in human, mouse and rat hearts. *J Mol Cell Cardiol* 2016;**98**:103–107.

31. Movassagh M, Choy M, Knowles DA, Simeoni I, Penkett C, Goddard M, Foo S. Distinct epigenomic features in end-stage failing human hearts. 2013;**124**: 2411–2422.

32. Iyer MK, Niknafs YS, Malik R, Singhal U, Sahu A, Hosono Y, Barrette TR, Prensner JR, Evans JR, Zhao S, Poliakov A, Cao X, Dhanasekaran SM, Wu Y-M, Robinson DR, Beer DG, Feng FY, Iyer HK, Chinnaiyan AM. The landscape of long noncoding RNAs in the human transcriptome. *Nat Genet* 2015;**47**:199–208.

33. Siggens L, Figg N, Bennett M, Foo R. Nutrient deprivation regulates DNA damage repair in cardiomyocytes via loss of the base-excision repair enzyme OGG1. *FASEB J* 2012;**26**:2117–2124.

34. Foo RSY, Chan LKW, Kitsis RN, Bennett MR. Ubiquitination and degradation of the anti-apoptotic protein ARC by MDM2. *J Biol Chem* 2007;**282**:5529–5535.

35. Ackers-johnson M, Li PY, Holmes AP, Brien SO, Pavlovic D, Foo RS. A simplified, Langendorff-free method for concomitant isolation of viable cardiac myocytes and non-myocytes from the adult mouse heart right ventricle. *Cardiovasc Res* 2016;**119**:909–920.

36. Matkovich SJ, Edwards JR, Grossenheider TC, Strong CDG, Ii GWD. Epigenetic coordination of embryonic heart transcription by dynamically regulated long noncoding RNAs. 2014;**111**:12264–12269.

37. Lian X, Hsiao C, Wilson G, Zhu K, Hazeltine LB, Azarin SM, Raval KK, Zhang J, Kamp TJ, Palecek SP. Robust cardiomyocyte differentiation from human pluripotent stem cells via temporal modulation of canonical Wnt signaling. *Proc Natl Acad Sci U S A* 2012;**109**:E1848–E1857.

38. Trapnell C, Roberts A, Goff L, Pertea G, Kim D, Kelley DR, Pimentel H, Salzberg SL, Rinn JL, Pachter L. Differential gene and transcript expression analysis of RNA-seq experiments with TopHat and Cufflinks. *Nat Protoc* 2012;**7**:562–578.

39. Gao Y, Wang J, Zhao F. CIRI: an efficient and unbiased algorithm for de novo circular RNA identification. *Genome Biol* 2015;**16**:4.

40. Li H, Durbin R. Fast and accurate short read alignment with Burrows–Wheeler transform. *Bioinformatics* 2009;**25**:1754–1760.

41. Jeck WR, Sharpless NE. Detecting and characterizing circular RNAs. *Nat Biotechnol* 2013;**18**:1199–1216.

42. Tompkins JD, Jung M, Chen C, Lin Z, Ye J, Godatha S, Lizhar E, Wu X, Hsu D, Couture LA, Riggs AD. EBioMedicine mapping human pluripotent-to-cardiomyocyte differentiation: methylomes, transcriptomes, and exon DNA methylation "memories." *EBIOM* 2016;**4**:74–85.

43. You X, Vlatkovic I, Babic A, Will T, Epstein I, Tushev G, Akbalik G, Wang M, Glock C, Quedenau C, Wang X, Hou J, Liu H, Sun W, Sambandan S, Chen T, Schuman EM, Chen W. Neural circular RNAs are derived from synaptic genes and regulated by development and plasticity. *Nat Neurosci* 2015;**18**:603–610.

44. Roberts AM, Ware JS, Herman DS, Schafer S, Baksi J, Bick AG, Buchan RJ, Walsh R, John S, Wilkinson S, Mazzarotto F, Felkin LE, Gong S, MacArthur JAL, Cunningham F, Flannick J, Gabriel SB, Altshuler DM, Macdonald PS, Heinig M, Keogh AM, Hayward CS, Banner NR, Pennell DJ, O'Regan DP, San TR, de Marvao A, Dawes TJW, Gulati A, Birks EJ, Yacoub MH, Radke M, Gotthardt M, Wilson JG, O'Donnell CJ, Prasad SK, Barton PJR, Fatkin D, Hubner N, Seidman JG, Seidman CE, Cook SA. Integrated allelic, transcriptional, and phenomic dissection of the cardiac effects of titin truncations in health and disease. *Sci Transl Med* 2015;**7**:270ra6.

45. Herman DS. Truncations of titin causing dilated cardiomyopathy. *N Engl J Med* 2013;**366**:619–628.

46. Ponting CP, Grant Belgard T. Transcribed dark matter: meaning or myth? *Hum Mol Genet* 2010;**19**:162–168.

47. Nigro JM, Cho KR, Fearon ER, Kern SE, Ruppert JM, Oliner JD, Kinzler KW, Vogelstein B. Scrambled exons. *Cell* 1991;**64**:607–613.

48. Werfel S, Nothjunge S, Schwarzmayr T, Strom T-M, Meitinger T, Engelhardt S. Characterization of circular RNAs in human, mouse and rat hearts. *J Mol Cell Cardiol* 2016;**98**:103–107.

49. Jakobi T, Czaja-hasse LF, Reinhardt R, Dieterich C. Profiling and validation of the circular RNA repertoire in adult murine hearts. *Genom Proteom Bioinf* 2016;**14**:216–223.

50. Li XF, Lytton J. A circularized sodium-calcium exchanger exon 2 transcript. *J Biol Chem* 1999;**274**:8153–8160.

51. Gualandi F, Trabanelli C, Rimessi P, Calzolari E, Toffolatti L, Patarnello T, Kunz G, Muntoni F, Ferlini A. Multiple exon skipping and RNA circularisation contribute to the severe phenotypic expression of exon 5 dystrophin deletion. *J Med Genet* 2003;**40**:e100.

52. Du WW, Yang W, Chen Y, Wu Z, Foster FS, Yang Z, Li X, Yang BB. Foxo3 circular RNA promotes cardiac senescence by modulating multiple factors associated with stress and senescence responses. *Eur Heart J* 2016; doi: 10.1093/eurheartj/ehw001.

53. Enuka Y, Lauriola M, Feldman ME, Sas-Chen A, Ulitsky I, Yarden Y. Circular RNAs are long-lived and display only minimal early alterations in response to a growth factor. *Nucleic Acids Res* 2016;**44**:1370–1383.

54. Denkinger MD, Leins H, Schirmbeck R, Florian MC, Geiger H. HSC aging and senescent immune remodeling. *Trends Immunol* 2015;**36**:815–824.

55. Burd CE, Jeck WR, Liu Y, Sanoff HK, Wang Z, Sharpless NE. Expression of linear and novel circular forms of an INK4/ARF-associated non-coding RNA correlates with atherosclerosis risk. *PLoS Genet* 2010;**6**:1–15.

56. Wang K, Long B, Liu F, Wang J-X, Liu C-Y, Zhao B, Zhou L-Y, Sun T, Wang M, Yu T, Gong Y, Liu J, Dong Y-H, Li N, Li P-F. A circular RNA protects the heart from pathological hypertrophy and heart failure by targeting miR-223. *Eur Heart J* 2016;**37**:2602–2611.

57. Conn SJ, Pillman KA, Toubia J, Conn VM, Salmanidis M, Phillips CA, Roslan S, Schreiber AW, Gregory PA, Goodall GJ. The RNA binding protein quaking regulates formation of circRNAs. *Cell* 2015;**160**:1125–1134.